Seismic Constraints on Damage Growth Within an Unstable Hanging Glacier

Author(s):
Chmiel, Malgorzata; Walter, Fabian Thomas; Pralong, Antoine; Preiswerk, Lukas; Funk, Martin; Meier, Lorenz; Brenguier, Florent

Publication date:
2023-05-16

Permanent link:
https://doi.org/10.3929/ethz-b-000614371

Originally published in:
Geophysical Research Letters 50(9), https://doi.org/10.1029/2022GL102007

Funding acknowledgement:
157551 - Glacial Hazard Monitoring with Seismology (GlaHMSeis) (SNF)

AGU ADVANCING EARTH AND SPACE SCIENCE

Geophysical Research Letters

RESEARCH LETTER
10.1029/2022GL102007

Seismic Constraints on Damage Growth Within an Unstable Hanging Glacier

Małgorzata Chmiel[1,2], Fabian Walter[1,2], Antoine Pralong[2], Lukas Preiswerk[2], Martin Funk[2], Lorenz Meier[3], and Florent Brenguier[4]

[1]Swiss Federal Institute for Forest, Snow and Landscape Research WSL, Zürich, Switzerland, [2]Laboratory of Hydraulics, Hydrology and Glaciology (VAW), ETH Zürich, Zürich, Switzerland, [3]Geoprevent AG, Zürich, Switzerland, [4]Université Grenoble Alpes, Institut des Sciences de la Terre, Grenoble, France

Key Points:

- In the months leading up to a break-off event, we find thousands of recurring icequakes on the Eiger hanging glacier in Switzerland
- Coda wave interferometry resolves displacements of icequake multiplets
- One multiplet displacement represents englacial damage corresponding to crevasse extension between unstable and stable ice masses

Supporting Information:

Supporting Information may be found in the online version of this article.

Correspondence to:

M. Chmiel,
malgorzata.chmiel@wsl.ch

Citation:

Chmiel, M., Walter, F., Pralong, A., Preiswerk, L., Funk, M., Meier, L., & Brenguier, F. (2023). Seismic constraints on damage growth within an unstable hanging glacier. *Geophysical Research Letters*, *50*, e2022GL102007. https://doi.org/10.1029/2022GL102007

Received 9 NOV 2022
Accepted 13 APR 2023

Author Contributions:

Conceptualization: Małgorzata Chmiel, Fabian Walter, Antoine Pralong, Lukas Preiswerk, Martin Funk, Lorenz Meier
Formal analysis: Małgorzata Chmiel
Investigation: Małgorzata Chmiel, Fabian Walter
Methodology: Małgorzata Chmiel, Lukas Preiswerk, Florent Brenguier
Software: Małgorzata Chmiel
Validation: Małgorzata Chmiel, Fabian Walter
Writing – original draft: Małgorzata Chmiel, Fabian Walter, Martin Funk
Writing – review & editing: Małgorzata Chmiel, Fabian Walter, Antoine Pralong, Lukas Preiswerk

Abstract Forecasting hanging glacier instabilities remain challenging as sensing technology focusing on the ice surface fails to detect englacial damage leading to large-scale failure. Here, we combine icequake cluster analysis with coda wave interferometry constraining damage growth on Switzerland's Eiger hanging glacier before a 15,000 m^3 break-off event. The method focuses on icequake migration within clusters rather than previously proposed "event counting." Results show that one cluster originated from the glacier front and migrated by 13.9(±1.2) m within 5 weeks before the break-off event. The corresponding crevasse extension separates unstable and stable ice masses. We use the measured source displacement for damage parametrization and find a 90% agreement between an analytical model based on damage mechanics and frontal flow velocities measured with an interferometric radar. Our analysis provides observational constraints for damage growth, which to date is primarily a theoretical concept for modeling englacial fractures.

Plain Language Summary Predicting the development of ice mass breaking off from unstable glaciers is challenging. Such glaciers are often located in remote places with steep terrain, making it difficult to gather observations. Because of that, our current view on ice damage development on unstable glaciers is incomplete. Here, we propose a new approach to tackle this problem using seismic observations from the Eiger hanging glacier in the Swiss Alps before a moderate 15,000 m^3 break-off event. We first group seismic signals according to their similarity. We then use waves scattered by fractures within the ice and at the glacier-rock boundaries to track displacement of ice damage. Our results suggest that a group of seismic signals is generated by crevasse propagation separating the unstable ice mass and the stable ice uphill. Combined with a simple analytical model, these observations indicate that seismic source displacement can be associated with damage propagation within unstable glacier ice. This is an important step toward a better understanding of unstable ice flow and forecasting glacier instabilities.

1. Introduction

Hanging glaciers are high-altitude glaciers that are inherently unstable and might produce catastrophic break-off events (Faillettaz et al., 2015). These glaciers are often partially frozen to their bedrock, allowing them to locate on steep slopes. Break-off events leading to substantial ice avalanches pose severe hazards to humans, settlements, and infrastructure in alpine terrain worldwide (e.g., Faillettaz et al., 2015; Tian et al., 2017).

Timely warnings and evacuation often remain the only solution to protect the population (Faillettaz et al., 2015). Good break-off forecasts are achieved with remote measurements of glacial surface velocities through ground-based radars capturing a power law acceleration before a break-off event (Faillettaz et al., 2008; Flotron, 1977; Pralong & Funk, 2006; Röthlisberger, 1977). Radar accuracy depends on atmospheric parameters and under ideal conditions mm-level displacements can be resolved, albeit with expensive deployments (Kienholz et al., 2021). Satellite imaging could provide an alternative, yet for break-off events involving water infiltration, warning signs from the glacier surface can be unnoticeable or difficult to interpret, as was the case for the recent ice avalanche from the Marmolada glacier in Italy (Lorenzo & Carlo, 2023).

Crevasse growth results from a combination of glacier geometry, ice rheology, subglacial hydrology, damage evolution, and basal motion (Faillettaz et al., 2015), which cannot be revealed with measurements of ice surface velocities only. These factors control the adhesion of ice to bedrock, cohesion with more stable up-slope ice, and shear strength to lateral abutments (Haeberli et al., 1989). Improved understanding of englacial processes leading

to crevasse growth through systematic observations is needed, especially in the context of climate change that might affect the stability of glaciers (e.g., Huggel, 2009; Kääb et al., 2018). A better comprehension of englacial damage accumulation would enhance prediction accuracy, extend forecasting lead-time, and improve risk mitigation strategies.

In the recent 1–2 decades, passive seismic measurements have become increasingly popular in glaciology (Podolskiy & Walter, 2016). They provide access to the interior and basal environments of glaciers and ice sheets: crevasse dynamics, basal sliding, subglacial water flow, and iceberg detachment are notoriously difficult to study with conventional glaciological techniques but can be monitored with seismometers at the ice surface (for an overview see, e.g., Aster & Winberry, 2017; Nanni et al., 2020; Podolskiy & Walter, 2016). For break-off events of steep glacial bodies, seismological research has so far focused on detecting "icequakes." This term is often used to refer to glacier-related microseismic events generated by glacier stick-slip motion (Caplan-Auerbach & Huggel, 2007; Weaver & Malone, 1979) and crack opening (Faillettaz, Funk, & Sornette, 2011; Faillettaz et al., 2008; Preiswerk et al., 2016). Beyond "icequake counting" analysis of seismic event locations or waveform attributes could reveal further details of source mechanisms and thus help characterize ice structural change leading to failure. This would allow testing theoretical predictions on the role of damage evolution (Pralong & Funk, 2006), basal sliding (Allstadt & Malone, 2014; Dalban Canassy et al., 2012, 2013), and external forcing, in particular climatic conditions (Faillettaz, Funk, & Sornette, 2011; Faillettaz, Sornette, & Funk, 2011).

Here, we study a hanging glacier's icequake signals focusing on later arriving seismic "coda" phases to quantify fracture development behind the ice front before a break-off event. We use seismic data from a 4-station network deployed on the Eiger hanging glacier in Switzerland between April and August 2016. We find over 200,000 recurring icequakes with substantial coda out of which we compile catalogs of 30 clusters each comprising events with high waveform similarities. Focusing on coda changes, we use the clusters to monitor source displacements that can be interpreted in terms of damage evolution as a preparation phase toward break-off events.

2. Study Site

The Eiger hanging glacier, located on the west face of the Eiger summit, Switzerland, extends from 3,500 to 3,200 m a.s.l. with a surface slope of 20° at the terminus (Figures 1a and 1b). The surface area of the Eiger hanging glacier was 0.08 km^2 in 2016 (Huss et al., 2013) with a mean and maximum thickness of about 40 and 70 m respectively (Margreth et al., 2017). The only study that performed temperature measurements of the Eiger hanging glacier determined englacial temperatures ranging between −5° and 0° and an average glacier flow velocity of 7 $m\,a^{-1}$ (Lüthi & Funk, 1997). The Eiger hanging glacier is polythermal, meaning that water coexists with glacier ice at the glacier base, except for the frontal part, which is cold and frozen to the bed (Lüthi & Funk, 1997). We refer the reader to Figure S1 and Text S1 in Supporting Information S1 for more details on the glacier's thermal regime. The glacier lies almost entirely in the accumulation zone, exhibiting a positive annual net surface balance. At the ice front, the glacier extent is limited by a topographic bedrock step, leading to a steep ice cliff from which periodic break-off events occur (Marchetti et al., 2021; Margreth et al., 2017; Raymond et al., 2003). Typical volumes of unstable ice are <10,000 m^3. The resulting ice avalanches are large enough to endanger hiking paths, ski infrastructure, and the train line that leads to Jungfraujoch, one of Europe's major tourist destinations (Figure 1a). In April 2016, a significant crevasse was observed behind the glacier front, indicating an impending break-off event (Figure S2 in Supporting Information S1). On the morning of 25 August 2016, an ice mass of 15,000 m^3 broke off the hanging glacier. This was the largest break-off event since 1991 (Margreth et al., 2017). The ice avalanche missed the Eigergletscher train station (Figure 1a) and came to rest 1,200 m vertically below the glacier.

3. Instrumentation

To warn against break-off events, a monitoring system has been operational next to the glacier since 2016, including an automatic camera (two photos per day of the glacier front) and an interferometric radar measuring the velocity of the glacier front (Meier et al., 2016). Between April and September 2016, the interferometric radar at the Eigergletscher train station recorded hourly line-of-sight velocity of the glacier front (Figures 1c and 1d).

Between April and August 2016, we installed four three-component Lennartz seismometers with natural frequency of 1 Hz on the glacier (Figure 1a) to monitor its icequake activity (Preiswerk, 2018; SED, 1985 for

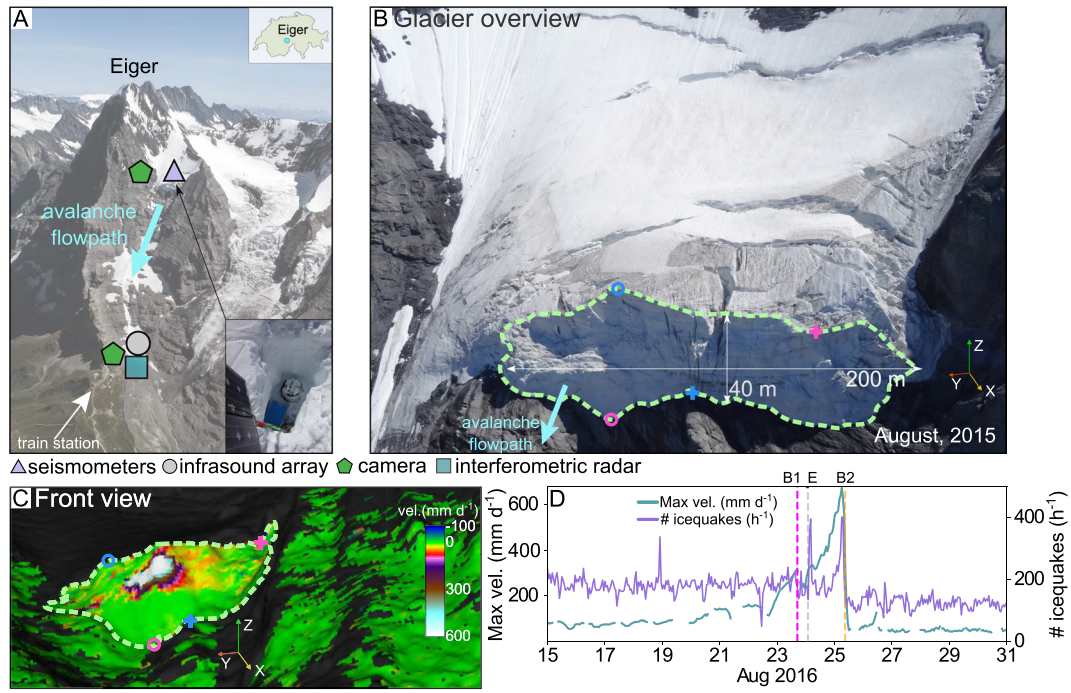

Figure 1. Study site: Eiger hanging glacier. (a) Instruments for glacier monitoring: infrasound array (gray circle, not operational during the break-off event), interferometric radar measuring glacier flow velocity (teal square), four 3-component seismometers (natural frequency: 1 Hz) installed on the glacier between April and August 2016 (stations EIG1-EIG4, purple triangle), an automatic camera targeting the unstable ice mass (green pentagons). Source: ETH-Bibliothek Zürich, Bildarchiv/Stiftung Luftbild Schweiz/Photograph: Swissair Photo AG/LBS_R2-010615/CC BY-SA 4.0. The insets show the location of Mount Eiger in Switzerland and a seismic station placed into a snow pit on a granite plate. The blue box contains the logger and battery. (b) The front of the Eiger hanging glacier in August 2015. (c) Line-of-sight velocity of the ice surface measured by the interferometric radar projected onto the digital elevation model of the glacier front (summed from 02:01 to 08:01 UTC, 25 August 2016). The area with maximum velocity identifies the ice portion about to collapse. A light green dashed line marks the outline of the glacier, and two color-coded crosses and two circles mark the same locations on the front in panels (b and c). (d) Temporal evolution of the maximum ice velocity and hourly icequake occurrence rate. Both curves are smoothed with a 1 hr moving average. The times of a small "B1" and the main "B2" break-offs and the M6.2 Amatrice earthquake "E" are represented in color-coded dashed vertical bars.

details on acquisition). Avalanches, snowfalls, and other factors associated with high altitude conditions challenge instrument maintenance on the glacier. However, station EIG2 recorded continuously for 4.5 months and up to three seismic stations operated simultaneously. Seismic data availability is shown in Figure S3 in Supporting Information S1. Our seismic stations recorded the main break-off on 25 August together with a precursory event on 23 August, the Amatrice earthquake of magnitude 6.2, and abundant icequake activity consisting of up to 400 events per hour (Figure 1d).

4. Methods

4.1. Catalog Compilation

We first determine overall icequake activity using a short-term average/long-term average (STA/LTA) algorithm with coincidence trigger over all available stations (Allen, 1978). Next, we divide icequake seismograms into clusters consisting of events with similar waveforms. In conventional seismological applications, waveform similarity is attributed to earthquake repeaters and multiplets that are closely spaced events with nearly identical source mechanisms (Poupinet et al., 1984). The cross-correlation coefficient between two seismograms is a measure of similarity and ranges between −1 and 1 with the latter corresponding to a perfect match. Repeaters have been defined as waveform pairs with a cross-correlation coefficient ≥0.9 (e.g., Uchida & Bürgmann, 2019). In glacial contexts, repeating icequakes have been linked to basal stick-slip beneath ice streams (e.g., Anandakrishnan & Bentley, 1993; Danesi et al., 2007; Smith, 2006; Zoet et al., 2012), Alpine valley glaciers (e.g., Gräff &

Walter, 2021; Helmstetter, Nicolas, et al., 2015; Walter et al., 2020), and glacier-covered volcanoes (e.g., Allstadt & Malone, 2014; Thelen et al., 2013). In contrast, multiplet seismograms have a lower cross-correlation coefficient ≥0.5 and in glacial environments have been associated with crevasse opening (Mikesell et al., 2012) and fracture propagation (Helmstetter, Moreau, et al., 2015).

We identify clusters of icequakes with similar waveforms prior to the break-off event by mutually cross-correlating STA/LTA detections within a sliding time window of 5 s using the Repeating Earthquake Detector in Python (RedPy, Hotovec-Ellis & Jeffries, 2016). For this step, we use icequakes coincidentally detected on stations EIG2 and EIG4 between 11 and 31 August 2016. EIG2 and EIG4 were the only stations working properly before the break-off event (station EIG4 was installed on 11 August 2016). We find over 200,000 repeating events with a correlation coefficient above 0.9 from which we choose the 30 clusters with more than 40 events (5% of all clusters). To extend our analysis over the entire monitoring period, we stack icequake waveforms within each cluster to form templates. Next, we search for similar icequakes with template matching against the continuous data recorded at the EIG2 station (e.g., Gibbons & Ringdal, 2006). For the implementation, we use the correlation-based Fast Match Filter (Beaucé et al., 2018), and we set the correlation coefficient threshold to 0.7. The threshold of 0.7 provides a comprehensive catalog that we need for coda wave measurements while rejecting events that potentially originate from different clusters. These steps leave us with 36,989 icequakes from 30 clusters, which we refer to as "multiplets" even though some icequake pairs may share cross-correlation coefficients above 0.9 (see Texts S2.1–S2.3 in Supporting Information S1 for details and Figure S4 in Supporting Information S1 for cluster waveform overview).

4.2. Coda Wave Interferometry

The later arriving coda waves are multiply scattered seismic signals that sample medium subvolumes multiple times by following more complex and longer paths than direct waves (Figure 2a, Figure S5 in Supporting Information S1). The resulting increased sensitivity of coda waves to medium changes is used in coda wave interferometry (CWI) to measure subtle changes in source locations, scatterer locations, and seismic velocities (e.g., Curtis et al., 2006; Sens-Schönfelder & Brenguier, 2019; Snieder et al., 2002). On Alpine glaciers with relatively little fracturing, CWI is challenging as homogeneous ice usually suppresses englacial scattering resulting in the weak coda, as shown in, for example, Sergeant et al. (2020) and Figure S6 in Supporting Information S1. However, pervasive fracturing on hanging glaciers generates substantial coda (Podolskiy & Walter, 2016) as confirmed by the seismograms at our study site (Figure 2b). For our icequake seismograms, we assume that coda changes are driven by perturbations in source locations and/or in ice elastic properties rather than by perturbations in scattering crevasse fields. This assumption is based on typical crevasse life times of up to 5 yr which are large compared to the monitoring period (Colgan et al., 2016) and on the high sensitivity of seismic velocities to changes in ice elasticity (Röthlisberger, 1972).

4.3. Cluster Location

We locate the source regions of each cluster in the glacier with Matched Field Processing, which exploits cross-array phase coherence of the wavefield recorded at a group of sensors by calculating the cross-spectral density matrix, CSDM (Kuperman & Turek, 1997). For each cluster and station, we stack icequake waveforms recorded on the vertical component when the station was working properly. This provides us with average waveform stacks for 2–4 stations depending on the cluster activity. We then use a 1.5 s long time window taken from the beginning of the stack that includes the highest-amplitude phase, which for frequencies above 1 Hz we assume is a Rayleigh wave (Deichmann et al., 2000). We perform a 2D grid search over northing and easting with spatial increments of 1 m using a simple Rayleigh wave propagation model in a homogeneous medium (v_R = 1,612 ms^{-1}, optimized in the range of 1,550–1,700 ms^{-1} with a velocity increment of 10 ms^{-1}). For each cluster, the maximum normalized MFP map indicates the optimal source back azimuth that maximizes the fit between the CSDM of the waveform stacks and the model (see Text S2.4 in Supporting Information S1 for details and Figures S7–S11 in Supporting Information S1).

4.4. Source Displacements

We now focus on the centroid displacement of icequake multiplets in each cluster. As detailed in Text S2.5 in Supporting Information S1, we furthermore estimate changes in the relative seismic velocity dv/v through CWI and coda wave attenuation (Figure S12 in Supporting Information S1). We first filter the seismograms of our 30 icequake clusters between 10 and 40 Hz and define a 1 s long coda window starting at 0.5 s after the direct arrival

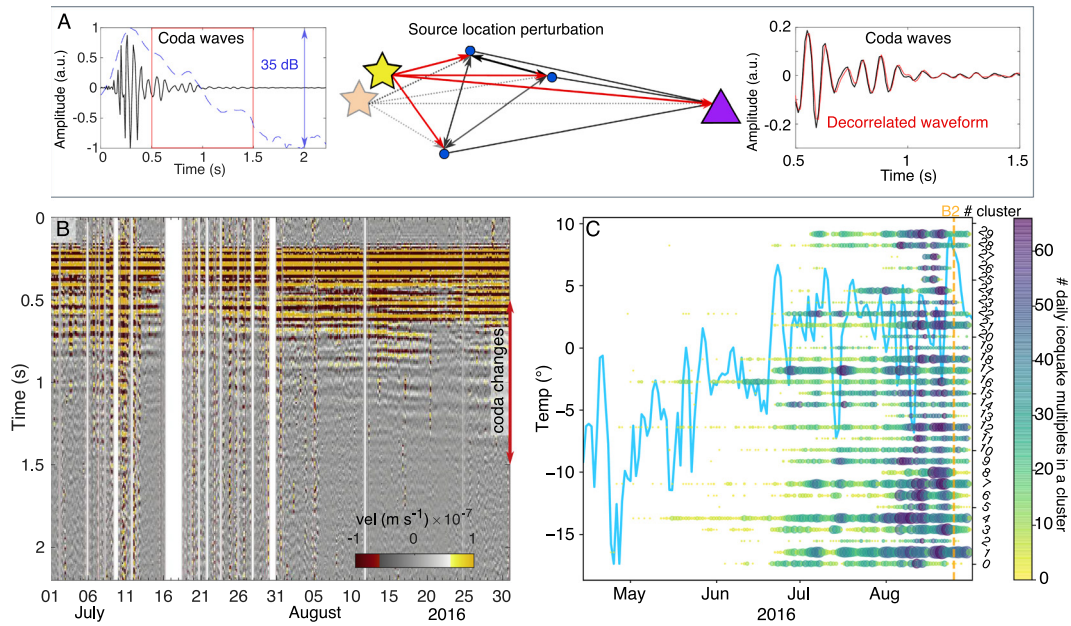

Figure 2. Coda wave interferometry and clusters of icequake multiplets. (a) The principle of source displacement measurements with coda wave interferometry (CWI). Left: Stack of icequakes within cluster 24 recorded on the vertical component of the EIG2 station. In red, we show the time window between $T_{min} = 0.5$ and $T_{max} = 1.5$ s that contains coda waves, and in blue the envelope decay in dB. Center: Illustration of a source location perturbation with a source (star), receiver (triangle), and a medium with point scatterers (circles). Direct and scattered ray paths are marked with solid red and black arrows, respectively. When the source position changes from the original to a perturbed location, some wave paths (dotted arrows) become longer while others become shorter and signals of these wave trajectories arrive earlier and later, respectively. We use the variance of the travel time changes to determine source displacements. Right: Coda waveforms before (black) and after the source perturbation (red). Based on Figure 1 in Singh et al. (2019). (b) Temporal variations of 4hr stacks of icequake multiplets in cluster 3 recorded on the vertical component of station EIG2. Time window (0.5–1.5) s used for CWI is marked with a red arrow. (c) Timeline showing daily activity of clusters. Daily occurrence is plotted as a circle on a line corresponding to its cluster. The color and size of each circle correspond to the average daily number of icequake multiplets. The cluster number is labeled on the right side. Air temperature measured at the MeteoSchweiz weather station Jungfraujoch is plotted as a blue line. The temperature is corrected by +1°C to account for the altitude of the Eiger hanging glacier, 3 km away. The main break-off "B2" is indicated as an orange dashed vertical bar.

associated with the surface wave (Figures 2a and 2b). To stabilize the measurement, we stack icequake signals within 4 hr windows after stacking up to three events per hour with the highest cross-correlation coefficient obtained from the template matching. As detailed in Section 4.2, we use CWI to measure a displacement between the centroids of icequake multiplets and invert for a continuous source displacement (Allstadt & Malone, 2014; Hotovec-Ellis & Jeffries, 2016). Since the measurements are not continuous, we use an L1 norm for regularization (e.g., Chmiel et al., 2018; Tibshirani, 1996) that enhances the solution sparsity.

5. Results

Between 5 August and the break-off event on 25 August 2016 the glacier front undergoes a clear acceleration from an average velocity of 4–5 cm day^{-1} to >60 cm day^{-1} (Figure 1d). After the main break-off on 25 August, the velocity drops below 10 cm day^{-1}. We observe an increase in the overall (non-clustered) seismicity rate only ~6 hr before the main break-off event to ~400 events hr^{-1} and a drop to 100 events hr^{-1} after the break-off. Before the small precursory break-off on 23 August, seismicity did not increase notably. On the other hand, our results show elevated seismicity 2 hr after the passing of the teleseismic waves of the M 6.2 Amatrice earthquake (e.g., Chiaraluce et al., 2017), around 01:00 UTC on 24 August. The 2 hr delay calls into question a direct relation to the earthquake's dynamic strain on the glacier ice. It does suggest that the detaching ice mass was still firmly attached, since the main break-off did not occur for another 31 hr. On longer time scales, we observe recurrent 1–2 hr long bursts of seismic activity, for example, on 18 August (Figure 1d). These bursts become ~10 times more frequent after 21 June when the air temperature exceeds 0°C and surface melt takes place at the glacier (Figure S13 in Supporting Information S1).

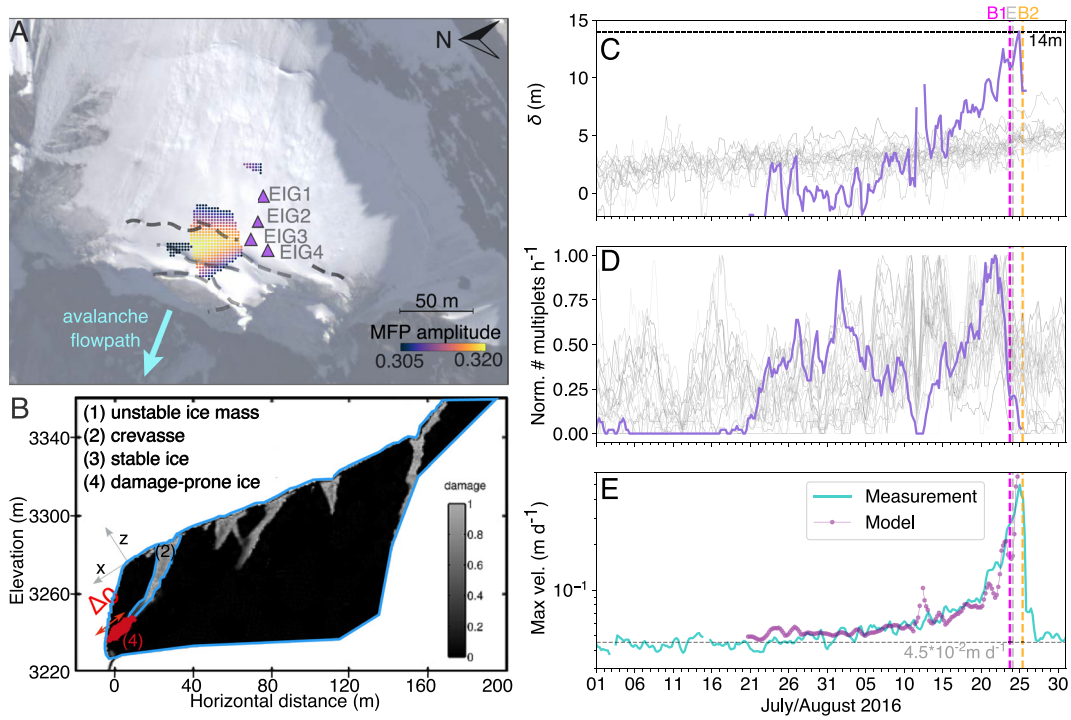

Figure 3. Analysis of clusters of icequake multiplets. (a) Two-dimensional map of average cluster locations obtained from matched-field processing (MFP) for the 10–40 Hz frequency range. We show only the top 95% of the resulting averaged MFP map. Background: orthophoto of the Eiger hanging glacier 1 day after the main break-off event. The positions of four seismic stations are marked with purple triangles. Main crevasses are marked with black dashed lines. Photo source: swisstopo flight, line 1308201608260940, 26 August 2016. (b) Damage model of the Eiger hanging glacier (reprinted with permission from Pralong & Funk, 2005 and annotated by the authors). Black represents ice without damage, and gray shading corresponds to the different values of damage. Glacier and the main crevasse are outlined in blue, and the red dots showing damage-prone ice are schematically indicated. (c) Displacements of icequake multiplet centroids δ and (d) icequake multiplet activity (normalized by the maximum number of events in the cluster). Cluster 24 is marked in purple and the other clusters are marked in gray. For each cluster, we represent the average source displacement over three components. (e) Zoom on the maximum velocity of the glacier front measured with the interferometric radar (in teal) and the frontal velocity calculated with Equation 2 (in purple). All measurements are smoothed with a 24 hr moving average. The small "B1" and the main "B2" break-offs, and the M 6.2 Amatrice earthquake "E" are represented in color-coded dashed vertical bars. The horizontal dashed line in Panel (c) denotes the maximum displacement of 14 m of cluster 24.

Twenty four out of the 30 clusters appear during the melt season, and the break-off events occur during elevated air temperature (Figure 2c). Twenty five clusters show their maximum activity 1–2 weeks before the break-off event, and nine clusters show decreasing activity after the break-off events. Two short-lived clusters (25 and 27) appear before the minor break-off event between 15 and 22 August. MFP is used to map the cluster origin location in space. Since we only have recordings from 2 to 4 stations that form a small aperture array, we cannot obtain focal-spot-like locations of clusters outside the array but only back azimuth information. Therefore, we produce an averaged MFP map reflecting the primary location where seismic energy is emitted by averaging the individual MFP maps as proposed by Chmiel et al. (2016), Lindner et al. (2020), and Retailleau et al. (2017). Before averaging, we limit the individual MFP maps at 1 wavelength distance (64 m, so twice the uncertainty caused by the diffraction limit) around the maximum location of the MFP map to focus on the main MFP map maximum within the glacier and minimize the effect of the spurious side lobes (Gal & Reading, 2019). Excluding source locations near the grid border (seven clusters) the averaged MFP analysis indicates the glacier front as the main source of seismic activity of our clusters (Figure 3a). However, it does not highlight other locations of seismic activity like the Bergschrund crevasse (Johnson, 1904), the highest point on the glacier where it begins to flow. See Figures S7–S11 in Supporting Information S1 and Text S2.4 in Supporting Information S1 for more details.

Using CWI, we track the migration of icequake multiplet centroids over time using a single station (Figure 3c and Figure S14 in Supporting Information S1). This pertains to displacement magnitude but not direction. We use cumulative differential displacement to quantify the total displacement (Equation 4 in Supporting Information S1).

Figure S15 in Supporting Information S1 shows histograms of the cumulative differential displacement of all clusters from 1 July to the main break-off event on 25 August 2016 and compares them to the glacier bulk displacement and station displacement. The bulk displacement of the glacier front in the stable regime measured by the interferometric radar can be estimated as ∼2.8 m per two months (∼4.5×10^{-2} m per day, Figure 3e). Stations EIG2 and EIG3 moved around 1.4 m between 6 June 2016 and 31 August 2016 (Preiswerk, 2018). Thus, ice flow transporting englacial seismic sources and seismic stations can partially explain the source displacement. However, more than half of the clusters (17 out of 30) migrated more than 3.8 m in two months, suggesting an additional migration mechanism. We propose that these cluster sources are extension events of crevasse tips. This explains an increase in cluster activity in spring when meltwater accumulates in crevasses and deepens them via hydrofracturing (e.g., Van der Veen, 1998). Among these clusters, cluster 24, which locates near the glacier front (Figure S7D in Supporting Information S1), forms an exception because its cumulative differential displacement amounts to 13.9(±1.2) m, between 20 July and 25 August when the cluster was active (Figures 3c and 3d, in purple).

6. Discussion

Faillettaz, Funk, and Sornette (2011) showed that on another hanging glacier located in the Swiss Alps, Weisshorn Glacier, the icequake activity accelerated together with the glacier front displacement ∼3 days before the failure of an unstable ice mass of volume ∼120,000 m^3. On the Eiger hanging glacier, icequake activity reacts after the main break-off event, showing only half of the event rate compared to pre-break-off times. However, simple icequake detections like in Faillettaz, Funk, and Sornette (2011) are of little use for break-off forecasting since they increase only within a few hours prior to a break-off event or not at all (Figure 1d). The difference in icequake activity at Weisshorn and the Eiger hanging glacier might be related to different geometries, the thermal regime at the glacier bed, the type of instability, and the volume of break-off events.

To our knowledge, icequake clusters have not been previously reported on hanging glaciers. Among the analyzed clusters, cluster 24 stands out, since it migrates at the highest and an accelerating rate and terminates its activity in the hours around the main break-off event (Figures 3c and 3d, cluster 24 is marked in purple). We argue that this cluster corresponds to the crevasse separating the unstable ice mass that detaches in the major break-off and the stable ice uphill for the following reason: (a) The activity of cluster 24 ceases after the major break-off. (b) MFP analysis locates cluster 24 toward the glacier front (Figure S7 in Supporting Information S1). (c) The source displacement of cluster 24 accelerates in parallel to the ice front velocity.

To explain the agreement between cluster displacement and front velocity quantitatively, we use the damage mechanics theory for ice rheology following Pralong et al. (2003). Damage D is a measure of the ice integrity, with $D = 0$ and $D = 1$ representing undamaged and fully damaged ice, respectively. Damage is assumed to only affect the viscosity of ice, not its rheology, and softening of increasingly damaged ice through a critical damage accumulation at the glacier's basal shear zone explains the pre-break-off acceleration of the glacier front (Pralong, 2006b).

To link our cluster 24 centroid displacement to frontal velocities we propose that

$$D = \frac{\Delta}{\Delta_0} \tag{1}$$

where Δ is the source displacement within cluster 24 and Δ_0 is the maximum displacement before the break-off taken as 14 m (marked with a dashed horizontal line in Figure 3c). With Equation 1 we parameterize the damage variable by the fraction of the ice connecting the unstable and stable glacier portions that is penetrated by the crevasse tip (Figure 3b). If this "ice bridge" is fully damaged, $\Delta = \Delta_0$ and hence $D = 1$, at which point the break-off occurs. We assume that D is measured toward the displacement direction x and it does not depend on the vertical coordinate z (see Figure 3b for coordinate system).

With the damage parameterization D in Equation 1 based on cluster centroid displacement δ we model the frontal velocity v_x of the unstable ice mass Pralong (2006b):

$$v_x = C A \sigma_{xz}^n \left[\frac{\Delta H}{(1-D)^n} + \frac{H}{n+1} \right] \tag{2}$$

where σ_{xz} is the xth and zth entry of the stress tensor, A and n are the flow rate factor and Glen's flow law exponent, respectively, H is the glacier thickness, ΔH is thickness of the active layer where damage develops, and C is an optimization constant.

Equation 2 is a simplified version of Equation 28 in Pralong (2006b), which for an infinitely long ice slab, describes the surface velocity as a result of damage accumulation within the basal shear layer together with conventional deformation of the ice column (second term, see Text S3 in Supporting Information S1 for details). We fit the first term of Equation 2 to the measured velocity optimizing for C and the exponent n. The canonical value of A depends on n and varies in literature (Paterson, 1999). For example, for remotely sensed deformation of Antarctic ice shelves, for a fit value of $n = 4$, Millstein et al. (2022), allow variations in flow rate factor A of 10 orders of magnitude compared to typical A values prescribed for $n = 3$, which are on the order of 10^{-25} Pa^{-3} s^{-1}.

Parameter C corrects the modeled glacier surface velocity for the variations in stress exponent and the idealized geometry of an infinite parallel-sided ice slab. We optimize C between 1 and 10^{14}. For n, we define the bounds as previously reported values of 1 and 4 (Cuffey & Paterson, 2010; Van der Veen, 1998). We specify the values used in the inversion in Table S1 in Supporting Information S1. The optimized value of the exponent is $n = 1.2$ and $C = 5.2 \times 10^{13}$.

The term describing the damage process $\frac{1}{(1-D)^n}$ in Equation 2 constrains the curvature of $v_x(t)$. For our fit $n = 1.2$ and the higher the value of n, the stronger the predicted curvature and the larger the deviation between the model and observations (Figure S16 in Supporting Information S1). In Text S3 in Supporting Information S1, we propose an alternative analytical model that assumes tensile damage, which seems more appropriate for crevasse opening near the ice front. However, that equation has the same form as Equation 2 and differs only by the numerator of the damage term.

The high agreement (90% calculated with the normalized residual sum of squares) between the analytical model and the measurement of the surface velocity indicates that seismology makes it possible to *directly* measure englacial damage. This also explains why the 13.9(±1.2) m cumulative differential displacement of cluster 24 is similar to the dimension of the fracture process zone, that is, the region where stress concentration ahead of a crevasse tip forms microcracks (Pralong, 2006a). Our measurements of englacial damage with seismic observations thus provide a direct metric on the integrity of the bulk ice mass. This can help assess whether a glacier is entering a critical regime before a break-off event. Importantly, the proposed seismic analysis provides indications for such a transition before surface measurements, because a pronounced increase in the displacement of cluster 24 started as early as 5 August 2023. Within about 1 week, a clear acceleration trend emerges (Figure 3c) while the elevated radar-derived surface velocities were still not apparent (Figure 3e). It took another week until the surface velocities entered a distinguishable power law acceleration mode on 21 August 2016.

7. Conclusion

Our study establishes a relation between englacial seismicity and the development of gravity-driven glacier instabilities. This approach seems superior to previously proposed analyses based on simple event detection, which in our case study did not identify seismic break-off precursors with comparable lead time.

The question of whether or not coda wave interferometry introduced here can provide new operational forecast tools has to be addressed with further measurements on different types of hanging glaciers. An enhanced sensor coverage that could be obtained with, for example, a distributed acoustic sensing system deployed at the glacier surface (Walter et al., 2020) could resolve the origin and the source mechanism of the multiplets better. The proposed approach can be also used to revisit existing seismic data to monitor fracture propagation on ice shelves, specifically, rift-like fractures that penetrate the entire ice thickness and can cause iceberg calving (e.g., Walker et al., 2013).

Our detection of englacial fracture dislocation establishes a more direct view of damage-related processes deep within a glacier compared to indirect damage manifestation of increased surface velocities. Thus, the presented approach constitutes a first-of-its-kind observational constraint on damage growth within glacier ice.

Data Availability Statement

Obspy Python routines (www.obspy.org, Beyreuther et al., 2010) were used to download waveforms and pre-process seismic data. REDPY can be downloaded from: https://github.com/ahotovec/REDPy/ (Hotovec-Ellis & Jeffries, 2016), and Fast Match Filter from https://github.com/beridel/fast_matched_filter/ (Beaucé et al., 2018). For source displacement, we used a modified MATLAB code package from Singh et al. (2019). The original MATLAB code package is available at https://github.com/JonathanSingh/cwi_codes/.
Seismometer data from stations EIG1, EIG2, EIG3, and EIG4 of the 4D local glacier seismology network (SED, 1985), http://networks.seismo.ethz.ch/networks/4d/ are archived at the Swiss Seismological Service http://www.fdsn.org/networks/detail/4D_1985/.

Interferometric radar data supporting this research are described in Margreth et al. (2017) and are available through the GRAVX online data portal of the company Geoprevent https://data.geoprevent.com with restrictions that include confidentiality agreement and are not accessible to the public or research community. To gain access, please contact Lorenz Meier (lorenz.meier@geoprevent.com) or info@geoprevent.com.

Acknowledgments
This work was funded by the Swiss National Science Foundation (SNSF) project Glacial Hazard Monitoring with Seismology (GlaHMSeis, Grant PP00P2_157551). The authors thank Editor Mathieu Morlighem, the anonymous reviewer, and Florent Gimbert for their helpful comments that allowed us to improve the manuscript. The authors thank John Clinton, Roman Racine, and Stefan Wiemer; the Swiss Seismological Service and its electronic laboratory (ELAB) for technical support and data archiving. The authors thank Geoprevent Ltd for allowing us to use their high-quality radar data and images. The authors thank Dominik Gräff, Amandine Sergeant, Andrew Curtis, Aurélien Mordret, and Guillaume Jouvet for helpful discussions.

References

Allen, R. V. (1978). Automatic earthquake recognition and timing from single traces. *Bulletin of the Seismological Society of America*, *68*(5), 1521–1532. https://doi.org/10.1785/bssa0680051521

Allstadt, K., & Malone, S. (2014). Swarms of repeating stick-slip icequakes triggered by snow loading at Mount Rainier volcano. *Journal of Geophysical Research: Earth Surface*, *119*(5), 1180–1203. https://doi.org/10.1002/2014jf003086

Anandakrishnan, S., & Bentley, C. R. (1993). Micro-earthquakes beneath Ice Streams B and C, West Antarctica: Observations and implications. *Journal of Glaciology*, *39*(133), 455–462. https://doi.org/10.1017/s0022143000016348

Aster, R., & Winberry, J. (2017). Glacial seismology. *Reports on Progress in Physics*, *80*(12), 126801. https://doi.org/10.1088/1361-6633/aa8473

Beaucé, E., Frank, W. B., & Romanenko, A. (2018). Fast Matched Filter (FMF): An efficient seismic matched-filter search for both CPU and GPU architectures. *Seismological Research Letters*, *89*(1), 165–172. https://doi.org/10.1785/0220170181

Beyreuther, M., Barsch, R., Krischer, L., Megies, T., Behr, Y., & Wassermann, J. (2010). ObsPy: A Python toolbox for seismology. *Seismological Research Letters*, *81*(3), 530–533. https://doi.org/10.1785/gssrl.81.3.530

Caplan-Auerbach, J., & Huggel, C. (2007). Precursory seismicity associated with frequent, large ice avalanches on Iliamna volcano, Alaska, USA. *Journal of Glaciology*, *53*(180), 128–140. https://doi.org/10.3189/172756507781833866

Chiaraluce, L., Di Stefano, R., Tinti, E., Scognamiglio, L., Michele, M., Casarotti, E., et al. (2017). The 2016 central Italy seismic sequence: A first look at the mainshocks, aftershocks, and source models. *Seismological Research Letters*, *88*(3), 757–771. https://doi.org/10.1785/0220160221

Chmiel, M., Roux, P., & Bardainne, T. (2016). Extraction of phase and group velocities from ambient surface noise in a patch-array configuration. *Geophysics*, *81*(6), KS231–KS240. https://doi.org/10.1190/geo2016-0027.1

Chmiel, M., Roux, P., Herrmann, P., Rondeleux, B., & Wathelet, M. (2018). Data-based diffraction kernels for surface waves from convolution and correlation processes through active seismic interferometry. *Geophysical Journal International*, *214*(2), 1468–1480. https://doi.org/10.1093/gji/ggy211

Colgan, W., Rajaram, H., Abdalati, W., McCutchan, C., Mottram, R., Moussavi, M. S., & Grigsby, S. (2016). Glacier crevasses: Observations, models, and mass balance implications. *Reviews of Geophysics*, *54*(1), 119–161. https://doi.org/10.1002/2015RG000504

Cuffey, K. M., & Paterson, W. S. B. (2010). *The physics of glaciers*. Academic Press.

Curtis, A., Gerstoft, P., Sato, H., Snieder, R., & Wapenaar, K. (2006). Seismic interferometry—Turning noise into the signal. *The Leading Edge*, *25*(9), 1082–1092. https://doi.org/10.1190/1.2349814

Dalban Canassy, P., Faillettaz, J., Walter, F., & Huss, M. (2012). Seismic activity and surface motion of a steep temperate glacier: A study on Triftgletscher, Switzerland. *Journal of Glaciology*, *58*(209), 513–528. https://doi.org/10.3189/2012JoG11J104

Dalban Canassy, P., Walter, F., Husen, S., Maurer, H., Faillettaz, J., & Farinotti, D. (2013). Investigating the dynamics of an Alpine glacier using probabilistic icequake locations: Triftgletscher, Switzerland. *Journal of Geophysical Research: Earth Surface*, *118*(4), 2003–2018. https://doi.org/10.1002/jgrf.20097

Danesi, S., Bannister, S., & Morelli, A. (2007). Repeating earthquakes from rupture of an asperity under an Antarctic outlet glacier. *Earth and Planetary Science Letters*, *253*(1), 151–158. https://doi.org/10.1016/j.epsl.2006.10.023

Deichmann, N., Ansorge, J., Scherbaum, F., Aschwanden, A., Bernard, F., & Gudmundsson, G. (2000). Evidence for deep icequakes in an Alpine glacier. *Annals of Glaciology*, *31*, 85–90. https://doi.org/10.3189/172756400781820462

Faillettaz, J., Funk, M., & Sornette, D. (2011). Icequakes coupled with surface displacements for predicting glacier break-off. *Journal of Glaciology*, *57*(203), 453–460. https://doi.org/10.3189/002214311796905668

Faillettaz, J., Funk, M., & Vincent, C. (2015). Avalanching glacier instabilities: Review on processes and early warning perspectives. *Reviews of Geophysics*, *53*(2), 203–224. https://doi.org/10.1002/2014rg000466

Faillettaz, J., Pralong, A., Funk, M., & Deichmann, N. (2008). Evidence of log-periodic oscillations and increasing icequake activity during the breaking-off of large ice masses. *Journal of Glaciology*, *54*(187), 725–737. https://doi.org/10.3189/002214308786570845

Faillettaz, J., Sornette, D., & Funk, M. (2011). Numerical modeling of a gravity-driven instability of a cold hanging glacier: Reanalysis of the 1895 break-off of Altelsgletscher, Switzerland. *Journal of Glaciology*, *57*(205), 817–831. https://doi.org/10.3189/002214311798043852

Flotron, A. (1977). Movement studies on a hanging glacier in relation with an ice avalanche. *Journal of Glaciology*, *19*(81), 671–672. https://doi.org/10.3189/s0022143000029592

Gal, M., & Reading, A. (2019). Beamforming and polarisation analysis. In *Seismic ambient noise* (pp. 188–217). Cambridge University Press. https://doi.org/10.1017/9781108264808.008

Gibbons, S. J., & Ringdal, F. (2006). The detection of low magnitude seismic events using array-based waveform correlation. *Geophysical Journal International*, *165*(1), 149–166. https://doi.org/10.1111/j.1365-246x.2006.02865.x

Gräff, D., & Walter, F. (2021). Changing friction at the base of an Alpine glacier. *Scientific Reports*, *11*(1), 10872. https://doi.org/10.1038/s41598-021-90176-9

Haeberli, W., Alean, J.-C., Müller, P., & Funk, M. (1989). Assessing risks from glacier hazards in high mountain regions: Some experiences in the Swiss Alps. *Annals of Glaciology*, *13*, 96–102. https://doi.org/10.3189/S0260305500007709

Helmstetter, A., Moreau, L., Nicolas, B., Comon, P., & Gay, M. (2015). Intermediate-depth icequakes and harmonic tremor in an Alpine glacier (Glacier d'Argentière, France): Evidence for hydraulic fracturing? *Journal of Geophysical Research: Earth Surface*, *120*(3), 402–416. https://doi.org/10.1002/2014jf003289

Helmstetter, A., Nicolas, B., Comon, P., & Gay, M. (2015). Basal icequakes recorded beneath an Alpine glacier (Glacier d'Argentière, Mont Blanc, France): Evidence for stick-slip motion? *Journal of Geophysical Research: Earth Surface*, *120*(3), 379–401. https://doi.org/10.1002/2014jf003288

Hotovec-Ellis, A. J., & Jeffries, C. (2016). Near real-time detection, clustering, and analysis of repeating earthquakes: Application to Mount St. Helens and Redoubt Volcanoes. In *Presented at Seismological Society of America Annual Meeting*.

Huggel, C. (2009). Recent extreme slope failures in glacial environments: Effects of thermal perturbation. *Annals of Glaciology*, *28*(11–12), 1119–1130. https://doi.org/10.5167/uzh-26255

Huss, M., Voinesco, A., & Hoelzle, M. (2013). Implications of climate change on Glacier de la Plaine Morte, Switzerland. *Geographica Helvetica*, *68*(4), 227–237. https://doi.org/10.5194/gh-68-227-2013

Johnson, W. D. (1904). The profile of maturity in Alpine glacial erosion. *The Journal of Geology*, *12*(7), 569–578. https://doi.org/10.1086/621181
Kääb, A., Leinss, S., Gilbert, A., Bühler, Y., Gascoin, S., Evans, S. G., et al. (2018). Massive collapse of two glaciers in western Tibet in 2016 after surge-like instability. *Nature Geoscience*, *11*(2), 114–120. https://doi.org/10.1038/s41561-017-0039-7
Kienholz, C., Rinerm, R., Graf, K., Tobler, D., Hählen, N., & Häberle, J. H. (2021). Monitoring and hazard management at the Spitze Stei rockslide (p. 1). Retrieved from https://fan-info.ch/wp-content/uploads/FAN-Agenda_21_1.pdf
Kuperman, W. A., & Turek, G. (1997). Matched field acoustics. *Mechanical Systems and Signal Processing*, *11*(1), 141–148. https://doi.org/10.1006/mssp.1996.0066
Lindner, F., Walter, F., Laske, G., & Gimbert, F. (2020). Glaciohydraulic seismic tremors on an Alpine glacier. *The Cryosphere*, *14*(1), 287–308. https://doi.org/10.5194/tc-14-287-2020
Lorenzo, O., & Carlo, B. (2023). Preliminary observation of Marmolada glacier collapse of July 2022 with space-based cameras. *Remote Sensing Letters*, *14*(1), 21–29. https://doi.org/10.1080/2150704X.2022.2152754
Lüthi, M. P., & Funk, M. (1997). Wie stabil ist der Hängegletscher am Eiger? *Spektrum der Wissenschaft*, *5*, 21–24.
Marchetti, E., Walter, F., & Meier, L. (2021). Broadband infrasound signal of a collapsing hanging glacier. *Geophysical Research Letters*, *48*(16), e2021GL093579. https://doi.org/10.1029/2021gl093579
Margreth, S., Funk, M., Tobler, D., Dalban, P., Meier, L., & Lauper, J. (2017). Analysis of the hazard caused by ice avalanches from the hanging glacier on the Eiger west face. *Cold Regions Science and Technology*, *144*, 63–72. https://doi.org/10.1016/j.coldregions.2017.05.012
Meier, L., Jacquemart, M., Blattmann, B., Wyssen, S., Arnold, B., & Funk, M. (2016). Radar-based warning and alarm systems for Alpine mass movements. In *Proceedings of the 13th Interpraevent Congress* (pp. 960–968).
Mikesell, T. D., van Wijk, K., Haney, M. M., Bradford, J. H., Marshall, H. P., & Harper, J. T. (2012). Monitoring glacier surface seismicity in time and space using Rayleigh waves. *Journal of Geophysical Research: Earth Surface*, *117*(F2). https://doi.org/10.1029/2011JF002259
Millstein, J. D., Minchew, B. M., & Pegler, S. S. (2022). Ice viscosity is more sensitive to stress than commonly assumed. *Communications Earth & Environment*, *3*(1), 57. https://doi.org/10.1038/s43247-022-00385-x
Nanni, U., Gimbert, F., Vincent, C., Gräff, D., Walter, F., Piard, L., & Moreau, L. (2020). Quantification of seasonal and diurnal dynamics of subglacial channels using seismic observations on an Alpine glacier. *The Cryosphere*, *14*(5), 1475–1496. https://doi.org/10.5194/tc-14-1475-2020
Paterson, W. S. B. (1999). *The physics of glaciers* (3rd ed.). Butterworth-Heinemannk.
Podolskiy, E., & Walter, F. (2016). Cryo-seismology. *Reviews of Geophysics*, *54*(4), 708–758. https://doi.org/10.1002/2016rg000526
Poupinet, G., Ellsworth, W. L., & Frechet, J. (1984). Monitoring velocity variations in the crust using earthquake doublets: An application to the Calaveras Fault, California. *Journal of Geophysical Research: Solid Earth*, *89*(B7), 5719–5731. https://doi.org/10.1029/JB089iB07p05719
Pralong, A. (2006a). Ductile crevassing. Glacier science and environmental change (pp. 317–318).
Pralong, A. (2006b). Oscillations in critical shearing, application to fractures in glaciers. *Nonlinear Processes in Geophysics*, *13*(6), 681–693. https://doi.org/10.5194/npg-13-681-2006
Pralong, A., & Funk, M. (2005). Dynamic damage model of crevasse opening and application to glacier calving. *Journal of Geophysical Research: Solid Earth*, *110*(B1), B01309. https://doi.org/10.1029/2004JB003104
Pralong, A., & Funk, M. (2006). On the instability of avalanching glaciers. *Journal of Glaciology*, *52*(176), 31–48. https://doi.org/10.3189/172756506781828980
Pralong, A., Funk, M., & Lüthi, M. P. (2003). A description of crevasse formation using continuum damage mechanics. *Annals of Glaciology*, *37*, 77–82. https://doi.org/10.3189/172756403781816077
Preiswerk, L. (2018). Monitoring and structural studies with glacier seismology, (Doctoral dissertation). ETH Zurich. https://doi.org/10.3929/ethz-b-000300505
Preiswerk, L., Walter, F., Anandakrishnan, S., Barfucci, G., Burkett, P. G., Dalban Canassy, P., et al. (2016). Monitoring unstable parts in the ice-covered Weissmies northwest face. In *13th Congress Interpraevent 2016*.
Raymond, M., Wegmann, M., & Funk, M. (2003). *Inventar gefährlicher gletscher in der schweiz, mitteilungen versuchsanstalt für wasserbau, hydrologie und glaziologie der eidgenössischen technischen hochschule zürich, vol. 182, versuchsanstalt für wasserbau*. ETH Zürich: Hydrologie und Glaziologie.
Retailleau, L., Landès, M., Gualtieri, L., Shapiro, N. M., Campillo, M., Roux, P., & Guilbert, J. (2017). Detection and analysis of a transient energy burst with beamforming of multiple teleseismic phases. *Geophysical Journal International*, *212*(1), 14–24. https://doi.org/10.1093/gji/ggx410
Röthlisberger, H. (1972). *Seismic exploration in cold regions*. Cold Regions Research and Engineering Laboratory.
Röthlisberger, H. (1977). Ice avalanche. *Journal of Glaciology*, *19*(81), 669–671. https://doi.org/10.3198/1977JoG19-81-669-671
SED. (1985). Temporary deployments in Switzerland associated with glacier monitoring; ETH Zurich. Other/Seismic Network [Dataset]. Swiss Seismological Service (SED) at ETH Zurich. https://doi.org/10.12686/sed/networks/4d
Sens-Schönfelder, C., & Brenguier, F. (2019). Noise-based monitoring. In N. N. L. Gualtieri, & A. Fichtner (Eds.), *Seismic ambient noise* (pp. 267–301). Cambridge University Press.
Sergeant, A., Chmiel, M., Lindner, F., Walter, F., Roux, P., Chaput, J., et al. (2020). On the Green's function emergence from interferometry of seismic wave fields generated in high-melt glaciers: Implications for passive imaging and monitoring. *The Cryosphere*, *14*(3), 1139–1171. https://doi.org/10.5194/tc-14-1139-2020
Singh, J., Curtis, A., Zhao, Y., Cartwright-Taylor, A., & Main, I. (2019). Coda wave interferometry for accurate simultaneous monitoring of velocity and acoustic source locations in experimental rock physics. *Journal of Geophysical Research: Solid Earth*, *124*(6), 5629–5655. https://doi.org/10.1029/2019JB017577
Smith, A. M. (2006). Microearthquakes and subglacial conditions. *Geophysical Research Letters*, *33*(24), L24501. https://doi.org/10.1029/2006GL028207
Snieder, R., Grêt, A., Douma, H., & Scales, J. (2002). Coda wave interferometry for estimating nonlinear behavior in seismic velocity. *Science*, *295*(5563), 2253–2255. https://doi.org/10.1126/science.1070015
Thelen, W. A., Allstadt, K., De Angelis, S., Malone, S. D., Moran, S. C., & Vidale, J. (2013). Shallow repeating seismic events under an alpine glacier at Mount Rainier, Washington, USA. *Journal of Glaciology*, *59*(214), 345–356. https://doi.org/10.3189/2013jog12j111
Tian, L., Yao, T., Gao, Y., Thompson, L., Mosley-Thompson, E., Muhammad, S., et al. (2017). Two glaciers collapse in western Tibet. *Journal of Glaciology*, *63*(237), 194–197. https://doi.org/10.1017/jog.2016.122
Tibshirani, R. (1996). Regression shrinkage and selection via the Lasso. *Journal of the Royal Statistical Society*, *58*(1), 267–288. https://doi.org/10.1111/j.2517-6161.1996.tb02080.x
Uchida, N., & Bürgmann, R. (2019). Repeating earthquakes. *Annual Review of Earth and Planetary Sciences*, *47*(1), 305–332. https://doi.org/10.1146/annurev-earth-053018-060119

Van der Veen, C. (1998). Fracture mechanics approach to penetration of surface crevasses on glaciers. *Cold Regions Science and Technology*, *27*(1), 31–47. https://doi.org/10.1016/s0165-232x(97)00022-0

Walker, C. C., Bassis, J. N., Fricker, H. A., & Czerwinski, R. J. (2013). Structural and environmental controls on Antarctic ice shelf rift propagation inferred from satellite monitoring. *Journal of Geophysical Research: Earth Surface*, *118*(4), 2354–2364. https://doi.org/10.1002/2013JF002742

Walter, F., Gräff, D., Lindner, F., Paitz, P., Köpfli, M., Chmiel, M., & Fichtner, A. (2020). Distributed acoustic sensing of microseismic sources and wave propagation in glaciated terrain. *Nature Communications*, *2436*(1), 2436. https://doi.org/10.1038/s41467-020-15824-6

Weaver, C. S., & Malone, S. D. (1979). Seismic evidence for discrete glacier motion at the rock-ice interface. *Journal of Glaciology*, *23*(89), 171–184. https://doi.org/10.3189/S0022143000029816

Zoet, L. K., Anandakrishnan, S., Alley, R. B., Nyblade, A. A., & Wiens, D. A. (2012). Motion of an Antarctic glacier by repeated tidally modulated earthquakes. *Nature Geoscience*, *5*(9), 623–626. https://doi.org/10.1038/ngeo1555

References From the Supporting Information

Aki, K., & Chouet, B. (1975). Origin of coda waves: Source, attenuation, and scattering effects. *Journal of Geophysical Research*, *80*(23), 3322–3342. https://doi.org/10.1029/jb080i023p03322

Chmiel, M., Roux, P., & Bardainne, T. (2019). High-sensitivity microseismic monitoring: Automatic detection and localization of subsurface noise sources using matched-field processing and dense patch arrays. *GEOPHYSICS*, *84*(6), KS211–KS223. https://doi.org/10.1190/geo2018-0537.1

Clarke, D., Zaccarelli, L., Shapiro, N. M., & Brenguier, F. (2011). Assessment of resolution and accuracy of the Moving Window Cross Spectral technique for monitoring crustal temporal variations using ambient seismic noise. *Geophysical Journal International*, *186*(2), 867–882. https://doi.org/10.1111/j.1365-246X.2011.05074.x

Fréchet, J., Martel, L., Nikolla, L., & Poupinet, G. (1989). Application of the cross-spectral moving-window technique (CSMWT) to the seismic monitoring of forced fluid migration in a rock mass. *International Journal of Rock Mechanics and Mining Sciences & Geomechanics Abstracts*, *26*(3), 221–233. https://doi.org/10.1016/0148-9062(89)91972-4

Gradon, C., Moreau, L., Roux, P., & Ben-Zion, Y. (2019). Analysis of surface and seismic sources in dense array data with match field processing and Markov chain Monte Carlo sampling. *Geophysical Journal International*, *218*(2), 1044–1056. https://doi.org/10.1093/gji/ggz224

Greve, R., & Blatter, H. (2009). *Dynamics of ice sheets and glaciers*. Springer Science & Business Media.

Hotovec-Ellis, A. J., Gomberg, J., Vidale, J. E., & Creager, K. C. (2014). A continuous record of intereruption velocity change at Mount St. Helens from coda wave interferometry. *Journal of Geophysical Research: Solid Earth*, *119*(3), 2199–2214. https://doi.org/10.1002/2013JB010742

Iken, A. (1988). Adaption of the hot-water-drilling method for drilling to great depth.

Jones, G., Kulessa, B., Doyle, S. H., Dow, C. F., & Hubbard, A. (2013). An automated approach to the location of icequakes using seismic waveform amplitudes. *Annals of Glaciology*, *54*(64), 1–9. https://doi.org/10.3189/2013AoG64A07

Mao, S., Campillo, M., van der Hilst, R. D., Brenguier, F., Stehly, L., & Hillers, G. (2019). High temporal resolution monitoring of small variations in crustal strain by dense seismic arrays. *Geophysical Research Letters*, *46*(1), 128–137. https://doi.org/10.1029/2018GL079944

Nanni, U., Gimbert, F., Roux, P., & Lecointre, A. (2021). Observing the subglacial hydrology network and its dynamics with a dense seismic array. *Proceedings of the National Academy of Sciences*, *118*(28). https://doi.org/10.1073/pnas.2023757118

Nanni, U., Roux, P., Gimbert, F., & Lecointre, A. (2022). Dynamic imaging of glacier structures at high-resolution using source localization with a dense seismic array. *Geophysical Research Letters*, *49*(6), e2021GL095996. https://doi.org/10.1029/2021GL095996

Pralong, A. (2005). On the instability of hanging glaciers, (Unpublished doctoral dissertation). ETH Zürich.

Snieder, R. (2004). Extracting the Green's function from the correlation of coda waves: A derivation based on stationary phase. *Physical Review E*, *69*(4), 046610. https://doi.org/10.1103/physreve.69.046610

Snieder, R., Duran, A., & Obermann, A. (2019). Locating velocity changes in elastic media with coda wave interferometry. In *Seismic ambient noise* (pp. 188–217). Cambridge University Press. https://doi.org/10.1017/9781108264808.008

Snieder, R., & Vrijlandt, M. (2005). Constraining the source separation with coda wave interferometry: Theory and application to earthquake doublets in the Hayward fault, California. *Journal of Geophysical Research: Solid Earth*, *110*(B4). https://doi.org/10.1029/2004JB003317

Walter, F., Clinton, J., Deichmann, N., Dreger, D. S., Minson, S., & Funk, M. (2009). Moment tensor inversions of icequakes on gornergletscher, Switzerland. *Bulletin of the Seismological Society of America*, *99*(2A), 852–870. https://doi.org/10.1785/0120080110

Walter, F., Deichmann, N., & Funk, M. (2008). Basal icequakes during changing subglacial water pressures beneath Gornergletscher, Switzerland. *Journal of Glaciology*, *54*(186), 511–521. https://doi.org/10.3189/002214308785837110

Walter, F., Roux, P., Röösli, C., Lecointre, A., Kilb, D., & Roux, P. (2015). Using glacier seismicity for phase velocity measurements and green's function retrieval. *Geophysical Journal International*, *201*(3), 1722–1737. https://doi.org/10.1093/gji/ggv069